UC Berkeley
UC Berkeley Previously Published Works

Title
Conformation of a single polyelectrolyte in poor solvents

Permalink
https://escholarship.org/uc/item/72z013v6

Journal
The Journal of Chemical Physics, 153(6)

ISSN
0021-9606

Authors
Duan, Chao
Li, Weihua
Wang, Rui

Publication Date
2020-08-14

DOI
10.1063/5.0017371

Peer reviewed

Conformation of a single polyelectrolyte in poor solvents

Chao Duan, Weihua Li (iD), and Rui Wang (iD)

View Online   Export Citation   CrossMark

Conformation of a single polyelectrolyte in poor solvents

View Online   Export Citation   CrossMark

Chao Duan,[1,2] Weihua Li,[2,a] (iD) and Rui Wang[1,3,b] (iD)

AFFILIATIONS

[1] Department of Chemical and Biomolecular Engineering, University of California Berkeley, Berkeley, California 94720, USA
[2] State Key Laboratory of Molecular Engineering of Polymers, Key Laboratory of Computational Physical Sciences, Department of Macromolecular Science, Fudan University, Shanghai 200433, China
[3] Materials Sciences Division, Lawrence Berkeley National Lab, Berkeley, California 94720, USA

[a] Electronic mail: weihuali@fudan.edu.cn
[b] Author to whom correspondence should be addressed: ruiwang325@berkeley.edu

ABSTRACT

Understanding the conformation of a polyelectrolyte (PE) is not only a fundamental challenge in polymer science but also critical for understanding the folding and aggregation of proteins. Here, we develop a theory by systematically including the electrostatic interactions into the self-consistent field theory for polymers to study the conformational behaviors of a single PE in poor solvents. As the backbone charge fraction of the PE increases, our theory predicts that the spherical globule (Sph) can either be elongated to a series of pearl-necklace (PN) structures or be flattened to two novel structures that have not been reported before: biconcave red cell and toroid. While the PN structures are stable conformations, the two fattened structures are metastable. We find that the cylindrical globule, the stability of which is under debate, is an unstable structure. The signature of the PN structures obtained by our calculation is less pronounced than that reported by other theoretical works due to the continuous change in the curvature from the pearl to the necklace, which, however, is in good agreement with the results from molecular simulations and neutron scattering experiments. In addition, our theory reveals different characteristics of the globule to PN transition: the transition from the Sph to the PN with double pearls is discontinuous, whereas those from adjacent PN structures are continuous at finite salt concentrations. Furthermore, we observe different scaling behaviors: the string width is not a constant as a thermal blob but decays as the backbone charge fraction increases.

I. INTRODUCTION

Polyelectrolytes (PEs) are polymers with charged repeating units, which have attracted widespread attention in both academic and industrial research.[1–4] Applications for PEs are ubiquitous, such as surfactants in a variety of personal care/health products,[5] surface-modifiers in water treatment and oil recovery,[6,7] additives in foods,[8,9] superabsorbers in agriculture and sanitation,[10] biomedical materials in implant coating and drug delivery,[11,12] and electrolytes in lithium batteries.[13,14] In addition, many biomacromolecules, like proteins, DNA, and RNA, are essentially PEs.[15] Due to the presence of long-range electrostatic interaction, PEs exhibit complex structural and dynamic behaviors.[16–23] Despite their fundamental importance and wide range of applications, PEs remain among the least understood systems in polymer science, in stark contrast with our understanding of neutral polymers.[24–27] The majority of PEs are composed of hydrocarbon backbones for which a polar medium such as water is a poor solvent. The addition of charged groups to polymer chains prevents aggregation and precipitation, thus significantly improving their solubility in aqueous solutions. A critical problem for almost all the solution properties of PEs is the conformation of a single polyelectrolyte chain in poor solvents. The study of PE conformation also provides fundamental understanding of the folding and aggregation of proteins, which is associated with many human disorders, including Alzheimer's, Parkinson's, and prion diseases.[28–30]

The competition between the electrostatic repulsion and the effective attraction induced by poor solvents leads to nontrivial

conformational behaviors of PEs, which has been a subject of long-standing debate.[31,32] Khokhlov suggested that a collapsed spherical globule cannot be stable as the charge density on the chain increases and would eventually deform into an elongated cylinder.[33] Based on the similarity between this problem and the Rayleigh instability of charged droplets, Kantor and Kardar further argued that the stable structure should not be cylindrical but pearl-necklace (PN)-like, which consists of highly stretched strings alternating with collapsed globules.[34–36] In addition, Dobrynin, Rubinstein, and Obukhov developed a scaling theory for this pearl-necklace model and predicted a cascade of abrupt transitions between necklaces with different numbers of pearls.[37] The pearl-necklace structure has been supported by AFM images[38–42] and molecular simulations of a polyelectrolyte in implicit solvents.[43–50] However, using molecular dynamics simulations either with an explicit solvent model or a solvent-accessible surface area model where the polymer–solvent interaction is rigorously considered, Yethiraj and co-workers claimed that the pearl-necklace structures were not clearly seen in the snapshots.[51,52] Instead, the polyelectrolyte shows structures similar to cylindrical globules in their simulations. This observation is also consistent with the lack of the pearl-necklace signature in the structure factor measured by small-angle neutron scattering (SANS).[41,53–56]

To reconcile the discrepancy between theories, simulations, and experiments, it is necessary to identify the stability of different candidate structures by accurately calculating the free energy. In addition, previous theories focused only on a few preassumed structures, which exclude the existence of other equilibrium structures beyond the cylindrical globule and the pearl-necklace.[37,57–59] Furthermore, motivated by the potential application of a PE as a soft single-chain nanoparticle and its essential connection with biomacromolecules, it is desirable to predict the response of the equilibrium conformation to external stimuli like solvent quality and ionic strength. It is also worthwhile to understand its dependence on the chain structure such as chain length, architecture, and charge distribution. In this work, we develop a theory to describe PE conformation in poor solvents. This theory systematically includes the electrostatics for charged systems and the self-consistent field theory (SCFT) for neutral polymers in a unified framework, which captures the coupling between charge interactions and chain conformation. Superior to existing theories, our work does not need to invoke any preassumed structure as *a priori*, not only providing the most accurate description of the density profile and free energy for known conformations but also facilitating the search for new equilibrium structures.

II. THEORY

As shown in Fig. 1, the system we considered is a subvolume V consisting of n_p monodisperse PE chains and n_s solvent molecules in the presence of n_+ mobile cations and n_- anions. $n_p = 1$ specifies a single PE chain. The subvolume is treated as a semicanonical ensemble:[60,61] the number of polymers in the subvolume is fixed while the solvent and mobile ions are connected with a bulk salt solution of an ion concentration $c_\pm^b$ that maintains the chemical potentials of the solvent μ_s and ions $\mu_\pm$. The PE is assumed to be a Gaussian chain of N Kuhn segments with a Kuhn length b. The smeared charge model is adopted to describe the charge distribution on the chain backbone
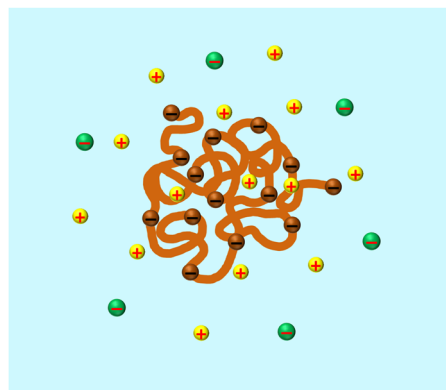

FIG. 1. Schematic of a single polyelectrolyte (PE) chain in poor solvents in the presence of mobile cations and anions.

such that the annealed fraction of segments α contains a charge with valency z_p.[62–68] While the choice of charge is arbitrary, we choose the charge on the PE backbone to be negative here. Mobile ions are taken as point charges with valency $z_\pm$.

The semicanonical partition function can be written as

$$\Xi = \frac{1}{n_p! v_p^{Nn_p}} \sum_{n_\gamma=0}^{\infty} \prod_\gamma \frac{e^{\mu_\gamma n_\gamma}}{n_\gamma! v_\gamma^{n_\gamma}} \prod_{i=1}^{n_p} \int \hat{D}\{\mathbf{R}_i\}$$
$$\times \prod_{j=1}^{n_\gamma} \int d\mathbf{r}_{\gamma,j} \prod_{\mathbf{r}} \delta[\hat{\phi}_p(\mathbf{r}) + \hat{\phi}_s(\mathbf{r}) - 1] \exp(-H), \quad (1)$$

where $\gamma = s, \pm$ represents all the small molecules in the system. v_p and v_γ are the volume of the chain segments and small molecules, respectively. For simplicity, we assume $v_p = v_s = v_0$. $\int \hat{D}\{\mathbf{R}_i\}$ denotes the integration over all chain configurations weighted by the Gaussian-chain statistics. $\hat{\phi}_p(\mathbf{r})$ and $\hat{\phi}_s(\mathbf{r})$ are the local instantaneous volume fraction of the solvent and the polymer, respectively. The δ functional accounts for the incompressibility. The Hamiltonian H in Eq. (1) is given by

$$H = \frac{\chi}{v_0} \int d\mathbf{r} \hat{\phi}_p(\mathbf{r})\hat{\phi}_s(\mathbf{r}) + \frac{1}{2} \int d\mathbf{r} \int d\mathbf{r}' \hat{\rho}_c(\mathbf{r}) C(\mathbf{r}, \mathbf{r}') \hat{\rho}_c(\mathbf{r}'), \quad (2)$$

which consists of two contributions: the short-range polymer–solvent interaction described by the Flory–Huggins χ parameter and the long-range Coulomb interaction between all charged species. $\hat{\rho}_c(\mathbf{r}) = z_+\hat{c}_+(\mathbf{r}) - z_-\hat{c}_-(\mathbf{r}) - z_p\alpha\hat{\phi}_p(\mathbf{r})/v_0$ is the local charge density, where $\hat{c}_\pm(\mathbf{r})$ is the instantaneous number density of ions. $C(\mathbf{r}, \mathbf{r}')$ is the Coulomb operator satisfying

$$-\nabla \cdot [\varepsilon(\mathbf{r})\nabla C(\mathbf{r}, \mathbf{r}')] = \delta(\mathbf{r} - \mathbf{r}'). \quad (3)$$

$\varepsilon(\mathbf{r}) = kT\varepsilon_0\varepsilon_r(\mathbf{r})/e^2$ is the scaled permittivity, where ε_0 is the vacuum permittivity and $\varepsilon_r(\mathbf{r})$ is the local dielectric constant which depends on the local composition of the system.[67–70]

We follow the standard self-consistent field approach[62] (see supplementary material Sec. I for the detailed derivation), which involves (1) identity transformation and Hubbard–Stratonovich

transformation to decouple the interacting system into noninteracting chains and ions in the fluctuating fields and (2) the saddle-point approximation to simplify the evaluation of the functional integral over the fluctuating fields. The free energy of the system is then

$$F = \frac{1}{v_0} \int d\mathbf{r} [\chi \phi_p (1 - \phi_p) - \omega_p \phi_p - \omega_s (1 - \phi_p)]$$
$$- \int d\mathbf{r} \left[c_+ + c_- - \frac{1}{2} \varepsilon (\nabla \psi)^2 + \frac{z_p \alpha}{v_0} \phi_p \psi \right]$$
$$- n_p \log Q_p + \log(n_p!) - e^{\mu_s} Q_s. \tag{4}$$

It should be noted that the free energy in Eq. (4) can also be perceived as the self-energy of a single polyelectrolyte chain for the case of $n_p = 1$.[71] Q_p is the single-chain partition function in the field ω_p, given by $Q_p = (1/v_0) \int d\mathbf{r}\, q(\mathbf{r}, N)$. $q(\mathbf{r}, s)$ is the chain propagator determined by the modified diffusion equation

$$\frac{\partial q(\mathbf{r}, s)}{\partial s} = \frac{b^2}{6} \nabla^2 q(\mathbf{r}, s) - \omega_p(\mathbf{r}) q(\mathbf{r}, s). \tag{5}$$

Q_s is the single particle partition function of the solvent in the field ω_s, given by $Q_s = (1/v_0) \int d\mathbf{r} \exp[-\omega_s(\mathbf{r})]$. The PE density profile ϕ_p, the ion concentration $c_\pm$, and the fields ω_p, ω_s, and ψ are determined by the following self-consistent equations:

$$\omega_p(\mathbf{r}) - \omega_s(\mathbf{r}) = \chi [1 - 2\phi_p(\mathbf{r})]$$
$$- \frac{\partial \varepsilon(\mathbf{r})}{\partial \phi_p(\mathbf{r})} v_0 [\nabla \psi(\mathbf{r})]^2 - z_p \alpha \psi(\mathbf{r}), \tag{6a}$$

$$\phi_p(\mathbf{r}) = \frac{n_p}{Q_p} \int_0^N ds\, q(\mathbf{r}, s) q(\mathbf{r}, N - s), \tag{6b}$$

$$1 - \phi_p(\mathbf{r}) = e^{\mu_s} \exp[-\omega_s(\mathbf{r})], \tag{6c}$$

$$- \nabla \cdot [\varepsilon(\mathbf{r}) \nabla \psi(\mathbf{r})] = z_+ c_+ - z_- c_-(\mathbf{r}) - \frac{z_p \alpha}{v_0} \phi_p(\mathbf{r}), \tag{6d}$$

$$c_\pm(\mathbf{r}) = \lambda_\pm e^{\mp z_\pm \psi(\mathbf{r})}, \tag{6e}$$

where $\lambda_\pm$ is the fugacity of the ions, defined as $\lambda_\pm = e^{\mu_\pm}/v_\pm$, which can be determined from the bulk salt concentration $c_\pm^b$.

Equations (6a)–(6e) are derived in the mean-field framework which cannot describe the effects of the spatially varying dielectric medium and the ion–ion correlation as a consequence of the fluctuation of the electrostatic field. To capture the local fluctuation effect, the Born solvation energy $u_\pm(\mathbf{r})$ can be included into the Boltzmann factor in Eq. (6e) as

$$c_\pm(\mathbf{r}) = \lambda_\pm e^{\mp z_\pm \psi(\mathbf{r}) - u_\pm(\mathbf{r})}, \tag{7}$$

where $u_\pm(\mathbf{r}) = z_\pm^2/[8\pi a_\pm \varepsilon(\mathbf{r})]$ with $a_\pm$ being the Born radius of cations and anions, respectively.[67,69,70] The inclusion of the Born solvation energy can be rigorously achieved by taking the Gaussian fluctuation of the electrostatic field and retaining the nonuniversal contribution in the length scale of the ion size. We refer interested

readers to the relevant literature for a more detailed derivation.[72,73] The Born solvation energy accounts for the electrostatic interaction between the ion and the local dielectric medium. For spatially varying ε, $u_\pm$ is not a constant, which cannot be adsorbed into the redefinition of the chemical potential and thus will affect the ion distribution.

By solving Eqs. (6a)–(6d) and (7) iteratively, the equilibrium density profile of the PE, the electrostatic field, and the ion distribution can be obtained. Based on the symmetry of possible structures, we use a cylindrical coordinate in the numerical calculation. Both the polymer density and the electrostatic potential field are set to be zero at the boundary of the cylindrical box. The approximate-factorization implicit (AFI) method is used to solve the modified diffusion equation [Eq. (5)], whereas the alternating-direction implicit (ADI) method is used to solve the Poisson–Boltzmann equation [Eq. (6d)].[74] Different initial seeds are used in the iteration process to generate all possible equilibrium structures. The free energy can be calculated from Eq. (4) to determine the stability of different equilibrium structures. Furthermore, the theory can be easily generalized to PEs with different chain architectures, chain statistics, and a variety of charge distributions on the backbone. Electrostatics beyond the mean-field level can also be straightforwardly included into the current theory by taking the Gaussian fluctuation around the saddle point.[72,73] While the current work focuses on the single chain conformation in the dilute limit, our theory can also be applied to study the aggregation behavior of multiple PE chains[75] for finite PE concentrations by including the effect of translational entropy in the framework of dilute solution thermodynamics.[60,61]

III. RESULTS AND DISCUSSION

In the current work, we focus on the effect of the backbone charge fraction α on the equilibrium structures of the PE and their transitions. Other effects such as polymer–solvent interaction, chain length, salt concentration, valency of ions, and dielectric contrast between the solvent and the polymer will be reported elsewhere. For simplicity, the dielectric constants of the polymer and the solvent are set to be the same ($\varepsilon_{r,p} = \varepsilon_{r,s} = 80$), yielding a constant Born solvation energy $u_\pm$ which can be adsorbed into a redefined chemical potential. The temperature is set to be 293 K, whereas the Bjerrum length $l_B = e^2/4\pi\varepsilon_0\varepsilon_r kT$ is 0.7 nm. The Kuhn length $b = 1.0$ nm. Both the backbone charge and the mobile ions are taken to be monovalent ($z_p = z_+ = z_- = 1$). The bulk salt concentration is set to be dilute ($c_\pm^b = 2 \times 10^{-3}$M) such that the Debye screening length $\kappa_D^{-1} = [4\pi l_B(z_+ c_+^b + z_- c_-^b)]^{-1/2} = 7$ nm, which is larger than the globule size, and the screening effect on the electrostatic interactions is not significant.

A. Equilibrium structures

The equilibrium structure of a PE in poor solvents is determined by the interplay between the electrostatic repulsion and the solvent-induced effective attraction between monomers. The charge fraction α has a great impact on the equilibrium shape, polymer density distribution, and electrostatic potential, as shown in Fig. 2. When α is small (e.g., $\alpha = 0.1$), the PE maintains a spherical globule (Sph) structure with a core region and a diffuse surface. In the
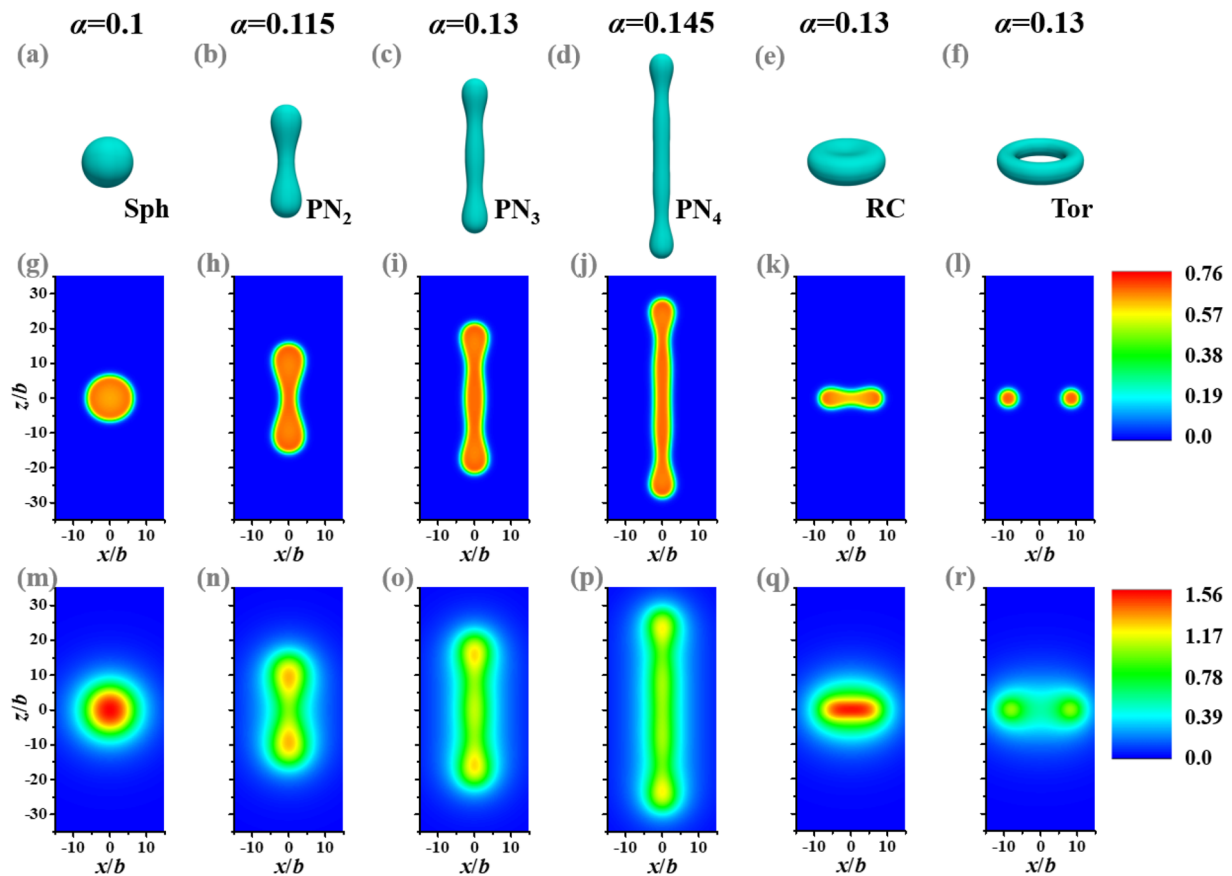
FIG. 2. Equilibrium structures formed by a single polyelectrolyte with different backbone charge fractions α in poor solvents. $N = 200$, $\chi = 1.0$, and $c_{\pm}^{b} = 2 \times 10^{-3}$ M. (a)–(f) show the 3D isosurface plots of the polymer density profiles of the spherical globule (Sph), pearl-necklace structures with two spheres (PN$_2$), three spheres (PN$_3$) and four spheres (PN$_4$), biconcave red cell (RC), and toroid (Tor) structures, respectively. (g)–(l) show the 2D visualizations in the xz plane of the polymer density distribution ϕ_p. The corresponding electrostatic potential distributions ψ of different equilibrium structures are shown in (m)–(r).

core region, the polymer density near the rim is slightly higher than that in the center [see Fig. 2(g) for the 2D density distribution and Fig. S1 for the radial density distribution in supplementary material Sec. II], benefiting the charge dispersion. This is different from the case of a charge neutral polymer in poor solvents where the polymer density is uniform in the entire globule core.[60,61] As shown in Fig. 2(m), charge accumulation in the globule core raises the electrostatic potential of the Sph. As α increases beyond a threshold value, the spherical shape can no longer be stable and have to deform, bearing similarity with the Rayleigh instability of a charged droplet.[34] The shape deformation is to release the electrostatic energy by increasing the average distance between charged monomers at the lowest cost of the surface energy due to the unfavorable contact between monomers and solvents. This deformation can be achieved by either elongating or flattening the spherical shape, as shown in Figs. 2(b)–2(d) and 2(e)–2(f), respectively. It should be noted that both the elongated structure and the flattened structure can exist at equilibrium for the same value of the charge fraction α, which are obtained by using different initial seeds in the iteration

process. To the best of our knowledge, flattened structures have not been reported before, despite a considerable discussion of elongated structures.[31,32]

For the elongated part, the equilibrium conformation of the PE shows a series of pearl-necklace (PN) structures with two pearls (PN$_2$), three pearls (PN$_3$), and four pearls (PN$_4$), as α increases to 0.115, 0.13, and 0.145, respectively. The change in the pearl structures is sensitive to the α values, which has also been observed in the early simulation of the PE with similar chain lengths.[37,44,47] The electrostatic repulsion increases as α becomes larger, leading to a more elongated PN structure. The number of pearls is identified from the local maxima of the distance between the axis of the symmetry and the Gibbs dividing surface (see supplementary material Sec. III for detailed description). Pearls are connected by thinner strings, whereas a large fraction of the mass and charge belong to the pearls, but the size of the chain is attributed to the stretch of the strings. While existing theories usually assumed in advance the exact different curvatures between the pearl and the string in the PN structure,[37,57–59] our theory generates the PN

structure without any prior assumption. Obviously, the change in the curvature from pearl to string is less significant than that considered by the scaling model and variational approach, especially for the PN structures with a large number of pearls. However, these PN structures obtained by our SCFT calculation are in good agreement with those observed in the snapshots of molecular simulations by Yethiraj *et al.*, where the polymer–solvent interaction is rigorously considered through an explicit solvent model or a solvent-accessible surface area model.[51,52] In their simulations, it is even difficult to distinguish the PN structures from the cylindrical globule due to thermal fluctuations. In addition, the density profiles show that the middle pears in PN_3 and PN_4 are notably smaller than the ending pearls, in agreement with the results from previous simulations.[43–51] However, it is clear that these pearls greatly deviate from the spherical shape, also strongly contradicting with the assumptions in the scaling model.[37] We also note that the PN structure becomes more pronounced as the solvent becomes poorer; i.e., the Flory–Huggins parameter χ becomes more positive. Furthermore, it is intriguing to note from the magnitude of ψ in Figs. 2(m)–2(p) that a PE with a larger backbone charge density can have a smaller electrostatic potential by increasing the number of pearls. This is in stark contrast with our intuition that the electrostatic potential usually increases with the amount of charge carried by the object. The effectiveness of the PN structure in releasing electrostatic energy also reveals the unique feature of the soft single-chain nanoparticles with shape regulation.

It has been long debated whether the cylindrical globule structure theoretically proposed by Khokhlov and observed in simulations is an equilibrium structure and whether this structure is more stable than the PN.[33,46,47,51,52] Our calculation demonstrates that the cylindrical globule structure cannot exist in equilibrium under the condition of dilute salt solution. Using an ellipsoid or a cylindrical globule as the initial condition of the polymer density profile, we find that these structures disappear during the iteration process when numerically solving the self-consistent equations and eventually transit to a more stable PN structure. It will be desirable to examine in the future whether the cylindrical structure can exist as a transition state in the kinetic pathway of the globule to pearl-necklace transition.

Our theory is free of any preassumption on the structure itself as invoked in existing theories, providing a facile way for searching new equilibrium structures which have not been reported before. As shown in Figs. 2(e) and 2(f), two flattened structures, biconcave red cell (RC) and toroid (Tor), can also be obtained for $\alpha = 0.13$, besides the elongated PN_3 structure. These flattened structures are in local minimum of the free energy since they can be obtained using different initial seeds in the iteration process of the numerical calculation and can be stabilized if small perturbations are introduced in the polymer density profile. The existence of RC and Tor as the equilibrium structure indicates that flattening the spherical shape besides elongation provides an alternative way to effectively disperse the charge. The strong accumulation of the electrostatic energy near the center of the spherical globule can be notably reduced in the biconcave shape through lowering the polymer density in the center region. The formation of the cavity in the Tor structure can further enlarge the separation between charges and thus lower the electrostatic potential, as shown in the comparison between Figs. 2(q) and 2(r). While the RC and Tor structures have been

experimentally observed in block copolymer micelles and lipid membranes,[76–78] here, it is predicted for the first time that these structures can also exist in the system of a single homogeneous PE chain. This indicates the essential similarity between the current system and other elastic soft matter systems. Furthermore, these versatile soft single-chain nanoparticles can be used as distinctive building blocks for the assembly of nanoporous materials.

B. Stability and conformational transition

By systematically including the electrostatic interactions and self-consistently describing the polymer density profile, our theory provides the accurate calculation of the free energy, which enables us to determine the stability of different equilibrium structures. Figure 3(a) shows the free energy (in excess of a charge-neutral polymer in the same salt solution) of different structures as a function of the charge fraction α in their existing regimes. While the Sph is stable for a small charge fraction, the PN is a more stable structure as α increases. The number of pearls in the stable structure increases with the increase in α. The two flattened structures, RC and Tor, which only exist in the intermediate regime of α, have a higher free energy than the PN structure and thus are metastable because the
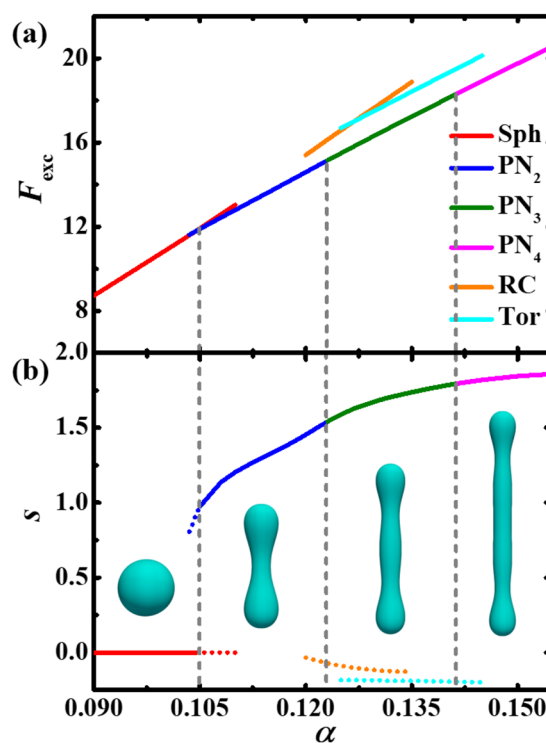

FIG. 3. Stability of different equilibrium structures and the conformational transition. (a) Excess free energy F_{exc} (based on a charge-neutral polymer in the same salt solution) as a function of the charge fraction α. The transition point from the Sph to PN_2 and the successive transitions from PN_m to PN_{m+1} ($m \geq 2$) are located by vertical dashed lines. (b) The plot of the order parameter of asphericity s, where the metastable regions of different structures are illustrated by dotted lines.

PN can be more effective in releasing the electrostatic repulsion due to the more diffusive polymer density distribution. This explains the fact that elongated PN structures are more likely to be observed than flattened structures in simulations and experiments.

The functional dependence of free energy on the charge fraction α shown in Fig. 3(a) also elucidates the order of the conformational transition between different stable structures. The scaling model and the variational approach predict that both the transition from the Sph to PN_2 and the successive transitions from PN_m to PN_{m+1} ($m \geq 2$) are discontinuous.[37,59] However, our theory predicts different characteristics of the globule to pearl-necklace transition compared to the existing theories. The transition from the Sph to PN_2 remains discontinuous due to the breaking of the spherical symmetry, which is clearly demonstrated by the crossing of the free energy curves belonging to these two structures at $\alpha = 0.105$, as shown in Fig. 3(a). Beyond this transition point, there are two metastable regimes corresponding to the Sph and PN_2. On the other hand, the free energy curves between different PN_m ($m \geq 2$) connect smoothly. The crossing point cannot be found in our calculation even when the accuracy of α was increased up to 10^{-4}. Our numerical results suggest that the transitions between successive pearl-necklace structures are continuous at finite salt concentrations, which contradicts with the prediction from existing theories. These different characteristics of conformational transition are due to the continuous change in the curvature from the pearl and the strings self-consistently generated in our theory. The existing theories enforce exact different curvatures between the pearl and string and further assume in advance a constant string width, which automatically gives rise to a cascade shape change in the transition from PN_m to PN_{m+1} when a new pearl appears from the string.[37,59] In contrast, the formation of the new pearl predicted by our theory is achieved by continuously adjusting the curvatures of the existing pearls and strings, which does not necessitate a discontinuous shape transition. The continuous change in the curvature in the conformational transition makes it difficult to identify the PN structures with a different number of pearls, in agreement with both the experimental results using an AFM image[38-42] as well as neutron scattering[41,53-56] and the snapshots observed in molecular simulations.[51,52]

The conformational transition can be more clearly illustrated by tracking the order parameter of asphericity, as shown in Fig. 3(b). The order parameter of asphericity s characterizes the deviation in the shape from a perfect sphere, which is defined as

$$s = \prod_{i=1}^{3} \frac{\lambda_i - \bar{\lambda}}{\bar{\lambda}}, \tag{8}$$

where λ_i ($i = 1, 2, 3$) are the three eigenvalues of the radius of gyration tensor $\mathbf{T}_{\alpha\beta}$ and $\bar{\lambda} = (\lambda_1 + \lambda_2 + \lambda_3)/3$. $\mathbf{T}_{\alpha\beta}$ can be calculated from the polymer density as

$$\mathbf{T}_{\alpha\beta} = \frac{\int d\mathbf{r} \int d\mathbf{r}' \phi_P(\mathbf{r}) \phi_P(\mathbf{r}') (r_\alpha - r'_\alpha)(r_\beta - r'_\beta)}{2[\int d\mathbf{r} \phi_P(\mathbf{r})]^2}, \tag{9}$$

with r_α being the αth Cartesian component of the position vector. s ranges from -0.25 to 2, where $s = 0$ corresponds to structures with a perfect spherical shape. The negative values of s correspond

to flattened structures like RC and Tor, whereas $s > 0$ are for elongated structures such as the PN with a different number of pearls. As shown in Fig. 3(b), s jumps abruptly from 0 to 0.9 at the Sph to PN_2 transition point, clearly demonstrating a discontinuous shape change. In contrast, s changes smoothly in the successive transitions from PN_m to PN_{m+1} ($m \geq 2$), which confirms the continuous nature of the transition between adjacent pearl-necklace structures, as we obtained from the free energy analysis.

C. Scaling behaviors

Since our theory shows different equilibrium structures and characteristics of conformational transition compared to existing theories, it is desirable to revisit the scaling behaviors of the pearl-necklace structure predicted previously. By assuming that the string is "long" (much longer than the pearls) and "narrow" (much thinner than the size of the pearls), the scaling model[37] and the subsequent modifications[59] predicted that the string has a constant width of a thermal blob, which is independent of the charge fraction α, whereas the pearls have the size of an electrostatic blob, scaling as $\alpha^{-2/3}$. However, these scaling behaviors are not fully confirmed by our results, as shown in Fig. 4. Figures 4(a) and 4(b) plot the α dependence of the string width d_{str} and the diameter of the pearls d_{pearl}, which are determined from the distance between the axis of the symmetry and the Gibbs dividing surface (see supplementary material Sec. III). It can be noted that d_{str} is comparable to d_{pearl}, particularly for middle pearls. This indicates that the assumption of "narrow string" is not valid for finite salt concentrations even though c^b used in the current calculation is very low. Due to the failure of the "narrow string" assumption, our results show that d_{str} changes nonmonotonically with α, which also contradicts with the constant string width predicted by the scaling theory.

To reconcile this discrepancy, we revisit the derivation of the scaling theory. Following the same procedure as the previous derivation by Dobrynin et al.[37] except invoking the "narrow string" assumption (see supplementary material Sec. IV), we obtain

$$d_{pearl} \sim b\tilde{l}_B^{-1/3} \alpha^{-2/3}, \tag{10a}$$

$$d_{str} \sim b\tilde{l}_B^{-1/3} \alpha^{-2/3}, \tag{10b}$$

$$L_{nec} \sim Nb\tilde{l}_B^{2/3} \alpha^{4/3}, \tag{10c}$$

where $\tilde{l}_B$ is the scaled Bjerrum length, $\tilde{l}_B = l_B/b = 1/(4\pi\varepsilon b)$. Equations (10a) and (10b) indicate that d_{str} is not a constant but decreases as α increases with the same scaling as d_{pearl}. As shown in Figs. 4(a) and 4(b), the $\alpha^{-2/3}$ dependence of both d_{str} and d_{pearl} is in good agreement with our numerical results in the regime of large α where PN structures are highly elongated such that the "long string" assumption becomes more accurate. In addition, the length of the PN, L_{nec}, is plotted in Fig. 4(c). The numerical result is closer to the newly derived scaling $L_{nec} \sim \alpha^{4/3}$, as shown in Eq. (10c), than the result $L_{nec} \sim \alpha$ obtained in the previous theory.[37] Equation (10c) also shows a linear dependence of L_{nec} on N under the condition of low salt concentration. Furthermore, the scaling of the critical value of the charge fraction α_c for the transition point from PN_{m-1} to PN_m ($m \geq 2$ and PN_1 stands for the spherical globule) will not be
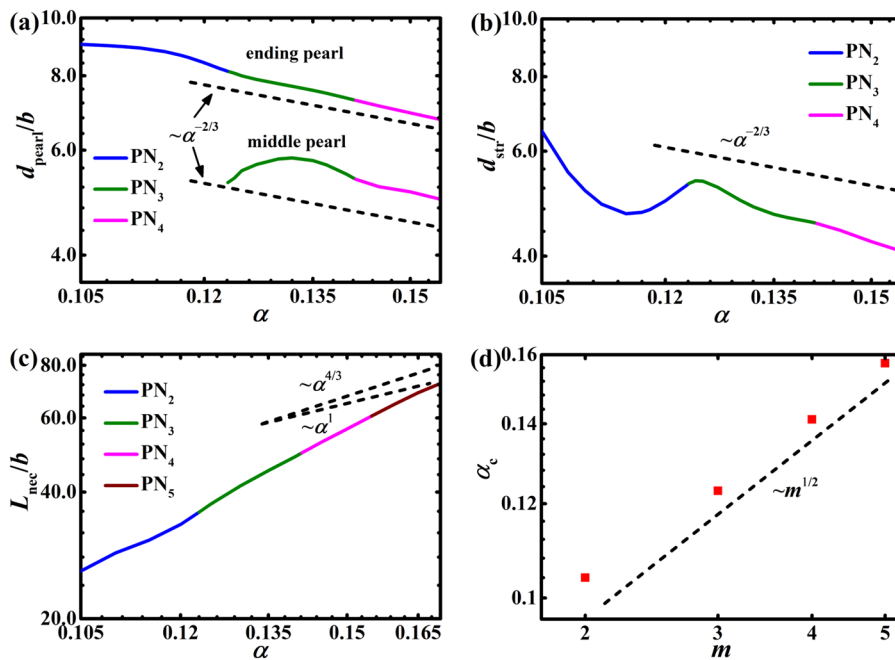
FIG. 4. Scaling behaviors of the pearl-necklace structure. The dependence of (a) the diameter of the pearls d_{pearl}, (b) the string width d_{str}, and (c) the length of the PN L_{nec} on the charge fraction α. For PN_3 and PN_4, the ending pearl and the middle pearl are plotted separately in (a). (d) The plot of the critical value of the charge fraction α_c for the transition point from PN_{m-1} to PN_m ($m \geq 2$ and PN_1 stands for the spherical globule).

affected by whether the "narrow string" assumption is invoked or not. Both our newly derived result and the previous theory show that $\alpha_c \sim m^{1/2}$. This scaling has been confirmed by our numerical results, as shown in Fig. 4(d), where the agreement becomes better as m increases.

D. Structure factor

Small-angle scattering techniques, such as SANS and small-angle x-ray scattering (SAXS), are the major tools for determining the single chain conformation because they provide direct measurement of the structure factor.[41,53–56] To facilitate the comparison with the scattering measurements, we examine the structure factors for different equilibrium structures predicted by our theory. Under the saddle-point approximation, the structure factor can be calculated based on the polymer density distribution $\phi_P(\mathbf{r})$ as

$$P(q) = \frac{\int d\mathbf{r} \int d\mathbf{r}' \phi_P(\mathbf{r}) \frac{\sin(q|\mathbf{r}-\mathbf{r}'|)}{q|\mathbf{r}-\mathbf{r}'|} \phi_P(\mathbf{r}')}{\left[\int d\mathbf{r} \phi_P(\mathbf{r})\right]^2}, \quad (11)$$

where q is the scattering wave number. Figure 5(a) shows the representative structure factors of the spherical globule (Sph), biconcave red cell (RC), and toroid (Tor). $P(q)$ for the Sph structure has a flat low-q part and a high-q part that decay as Porod's law q^{-4}. The strong oscillations at higher-q values indicate that the globule has a sharp surface and does not fluctuate significantly. The RC structure has a similar scattering behavior as the oblate disk except for two shoulders in the intermediate-q regime which indicates the signature of the concavity. The two shoulders at $q \approx 0.64b^{-1}$ and $q \approx 1.07b^{-1}$ correspond to the diameter of the disk ($\approx 9.8b$) and the

width of the thickest point ($\approx 5.9b$), respectively. In addition, $P(q)$ for the Tor structure also shows typical characteristics of an oblate body in the low-q part; on the other hand, the two shoulders in the intermediate-q regime (i.e., $q \approx 0.52b^{-1}$ and $q \approx 0.94b^{-1}$) correspond to the size of the central hole ($\approx 12b$) and the width of the torus ring ($\approx 6.7b$), respectively.

The structural factors of a series of elongated PN structures are shown in Fig. 5(b), which can be divided into three different regimes: the Guinnier regime at $qR_g \leq 1$, where R_g is the radius of gyration, characterizing the size of the PE chain as a whole; the q^{-1} regime at intermediate-q values, elucidating the stretched chain conformation overall as an elongated cylinder in this length scale; and the Porod regime at a high-q range, where $P(q) \sim q^{-4}$, indicating the approximate spherical shape of individual pearls. The signature of the PN structure is the existence of shoulders in the q^{-1} regime as a result of the inter-pearl scattering.[46,47,79] The number of pearls in the PN structure can be identified by the number of shoulders plus one, whereas the corresponding q values of the shoulders reflect the pearl–pearl distances.[46,47,79] Taking PN_3 as an example, the first shoulder at $q \approx 0.23b^{-1}$ can be assigned to the distance between two ending pearls ($\approx 27b$), and the second shoulder at $q \approx 0.38b^{-1}$ can be assigned to the distance between the ending pearl and its adjacent middle pearl ($\approx 17b$). The pearl–pearl distances found from the structure factors in Fig. 5 are in agreement with the results obtained from the density profiles in Fig. 2. Furthermore, it can be noted in Fig. 5(b) that the shoulders become less pronounced as the number of pearls increases, in accordance with the less distinguishable structure between the pearls and strings as illustrated in Fig. 2. This also provides an explanation of the difficulty in the neutron scattering experiment to unambiguously identify the PN structure especially when the number of pearls is large.
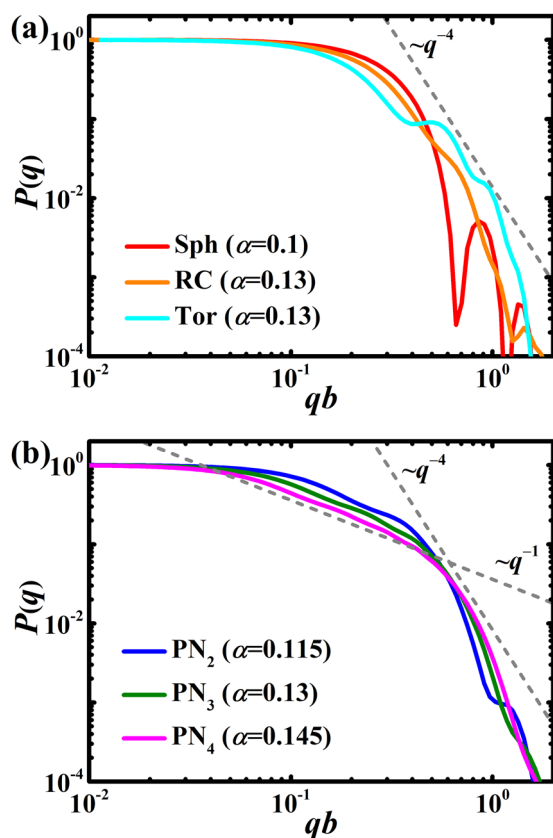
FIG. 5. Plot of the structure factors $P(q)$ as a function of the wave number q (in the unit of b^{-1}) for different equilibrium structures: (a) spherical globule (Sph), biconcave red cell (RC), and toroid (Tor) and (b) pearl-necklace structures with two spheres (PN$_2$), three spheres (PN$_3$), and four spheres (PN$_4$). The dashed lines indicate an elongated cylinder with $P(q) \sim q^{-1}$ and Porod scattering for a sphere with $P(q) \sim q^{-4}$.

Another difficulty for the PN to be experimentally identified is the fluctuation effects, such as the polydispersity, nonuniform line charge distribution, shape and size of pearls and strings, and the number of pearls, which will broaden and overlap characteristic signatures. It should be noted that our current calculation is in the framework of self-consistent field theory (SCFT) which neglects the fluctuation of density and electrostatic fields. The equilibrium structures obtained is valid under the condition that the surface energy is much larger than kT; otherwise, shape fluctuation must be taken into account. This condition is equivalent to the requirement that the number of thermal blobs within the structure must be much larger than one.[26] Particularly, the characteristic signature of the PN will be highly blunted if the widths of the string and the globule are reduced to the thermal blob size. It will be difficult to identify the number of pearls, and the dumbbell structure (PN$_2$) will be the most pronounced. Although the study of the fluctuation effect is beyond the scope of the current work, it will be interesting to include this effect in the future.

IV. CONCLUSIONS

In this work, we have developed a theory which systematically includes the electrostatic interactions into the self-consistent field theory (SCFT) for polymer systems to study the conformation of a single polyelectrolyte in poor solvents. This theory calculates the free energy of different equilibrium structures accurately, facilitating the determination of the stable conformations and their transition. As the backbone charge fraction α increases, the theory predicts that the spherical globule can either be elongated to a series of pearl-necklace structures or be possibly flattened to a biconcave red cell structure and a toroid structure. This is the first time the existence of flattened structures for a single homogeneous PE chain is reported. While the pearl-necklace structures are stable conformations, the two flattened structures are metastable. Our calculation demonstrates that the cylindrical globule, a structure of long-standing debate in the literature, cannot exist in equilibrium. Without preassuming different curvatures from the pearl to the string, the signature of the pearl-necklace structures obtained by our calculation is less pronounced than that predicted by existing theories, which, however, is in good agreement with both the molecular simulations using explicit solvents and the neutron scattering experiments. Our theory also shows that the pearl-necklace structure with a larger backbone charge fraction can have a smaller electrostatic potential through increasing the number of pearls, indicating the unique shape regulation of these smart single-chain nanoparticles. In addition, our theory elucidates different characteristics of the globule to pearl-necklace transition compared to existing theories: the transition from the Sph to PN$_2$ is discontinuous, whereas the successive transitions from PN$_m$ to PN$_{m+1}$ ($m \geq 2$) are continuous at finite salt concentrations. Furthermore, our theory shows different scaling behaviors compared to existing theories due to the failure of the "narrow string" approximation. The string width is not a constant as a thermal blob but decays as $\alpha^{-2/3}$.

Although we have only studied the conformation of a homogeneous PE chain in a monovalent salt solution in the current work, the theory developed here can be easily generalized to PEs with different chain architectures and statistics, a variety of backbone charge distributions and systems with more complex electrostatics beyond the mean-field framework. This theoretical platform is able to predict the response of the soft single-chain nanoparticle to a variety of external stimuli, including solvent quality, dielectric medium, ion concentration, valency, and tensile forces.[80] The flattened biconcave red cell and toroid structures reported in this work also reveal the possibility that other novel structures may exist in certain external conditions, which can be further fine-tuned through designing the chain structure. The density profiles and free energies of a single-chain soft particle and multiple-chain clusters obtained from the current calculation in the semicanonical ensemble can also be included into the dilute solution thermodynamics to study the aggregation behaviors of polyelectrolytes.[60,61] The theory-aided design of smart nanoparticles will greatly broaden the applications of PEs in sensors, drug-delivery vehicles, and nanoporous materials. Furthermore, the theoretical platform developed here facilitates the study of a wealth of structure, interfacial, and dynamic behaviors of polyelectrolytes, which will provide a fundamental step toward understanding challenges in protein systems, such as folding, binding, aggregation, and translocation.

SUPPLEMENTARY MATERIAL

See the supplementary material for the derivation of the self-consistent field theory for polyelectrolyte solutions, radial density distribution of the spherical globule, characteristic lengths of the pearl-necklace structure, and revisiting the derivation of the scaling relations for the pearl-necklace structure.

ACKNOWLEDGMENTS

DATA AVAILABILITY

The data that support the findings of this study are available within the article and its supplementary material.

REFERENCES

[1] S. Förster and M. Schmidt, Adv. Polym. Sci. **120**, 51 (1995).

[2] C. Holm, M. Rehahn, W. Oppermann, and M. Schmidt, *Polyelectrolytes with Defined Molecular Architecture II* (Springer-Verlag Berlin Heidelberg, 2004).

[3] M. Müller, *Polyelectrolyte Complexes in the Dispersed and Solid State II: Application Aspects* (Springer-Verlag Berlin Heidelberg, 2014).

[4] M. Muthukumar, Macromolecules **50**, 9528 (2017).

[5] L. D. Rhein, M. Schlossman, A. O'Lenick, and P. Somasundaran, *Surfactants in Personal Care Products and Decorative Cosmetics* (CRC Press, 2006).

[6] D. A. Z. Wever, F. Picchioni, and A. A. Broekhuis, Prog. Polym. Sci. **36**, 1558 (2011).

[7] K. He, H. Duan, G. Y. Chen, X. Liu, W. Yang, and D. Wang, ACS Nano **9**, 9188 (2015).

[8] C. Schmitt and S. L. Turgeon, Adv. Colloid Interface Sci. **167**, 63 (2011).

[9] A. P. Steinberg and Z.-G. Wang, Biomacromolecules **20**, 2675 (2019).

[10] T. Oya, T. Enoki, A. Y. Grosberg, S. Masamune, T. Sakiyama, Y. Takeoka, K. Tanaka, G. Wang, Y. Yilmaz, M. S. Feld, R. Dasari, and T. Tanaka, Science **286**, 1543 (1999).

[11] N. J. Shah, M. N. Hyder, M. A. Quadir, N.-M. Dorval Courchesne, H. J. Seeherman, M. Nevins, M. Spector, and P. T. Hammond, Proc. Natl. Acad. Sci. U. S. A. **111**, 12847 (2014).

[12] S. Roy, N. M. Elbaz, W. J. Parak, and N. Feliu, ACS Appl. Bio Mater. **2**, 3245 (2019).

[13] D. T. Hallinan and N. P. Balsara, Annu. Rev. Mater. Res. **43**, 503 (2013).

[14] J. Mindemark, M. J. Lacey, T. Bowden, and D. Brandell, Prog. Polym. Sci. **81**, 114 (2018).

[15] G. C. L. Wong and L. Pollack, Annu. Rev. Phys. Chem. **61**, 171 (2010).

[16] M. Rubinstein and R. H. Colby, Phys. Rev. Lett. **73**, 2776 (1994).

[17] Q. Liao, A. V. Dobrynin, and M. Rubinstein, Macromolecules **36**, 3386 (2003).

[18] P.-Y. Hsiao and E. Luijten, Phys. Rev. Lett. **97**, 148301 (2006).

[19] A. M. Tom, S. Vemparala, R. Rajesh, and N. V. Brilliantov, Phys. Rev. Lett. **117**, 147801 (2016).

[20] K. Grass, U. Böhme, U. Scheler, H. Cottet, and C. Holm, Phys. Rev. Lett. **100**, 096104 (2008).

[21] S. Fischer, A. Naji, and R. R. Netz, Phys. Rev. Lett. **101**, 176103 (2008).

[22] M. Muthukumar, Proc. Natl. Acad. Sci. U. S. A. **113**, 12627 (2016).

[23] D. Jia and M. Muthukumar, J. Am. Chem. Soc. **141**, 5886 (2019).

[24] P. G. de Gennes, *Scaling Concepts in Polymer Physics* (Cornell University Press, Ithaca, 1979).

[25] M. Doi and S. F. Edwards, *The Theory of Polymer Dynamics* (Oxford University Press, New York, 1994).

[26] M. Rubinstein and R. H. Colby, *Polymer Physics* (Oxford, 2003).

[27] Z.-G. Wang, Macromolecules **50**, 9073 (2017).

[28] V. S. Pande, A. Y. Grosberg, and T. Tanaka, Rev. Mod. Phys. **72**, 259 (2000).

[29] E. Shakhnovich, Chem. Rev. **106**, 1559 (2006).

[30] V. Munoz, *Protein Folding, Misfolding and Aggregation* (RSC, 2008).

[31] A. Dobrynin and M. Rubinstein, Prog. Polym. Sci. **30**, 1049 (2005).

[32] A. Dobrynin, Curr. Opin. Colloid Interface Sci. **13**, 376 (2008).

[33] A. R. Khokhlov, J. Phys. A: Math. Gen. **13**, 979 (1980).

[34] Lord Rayleigh, Philos. Mag. **14**, 184 (1882).

[35] Y. Kantor and M. Kardar, Europhys. Lett. **27**, 643 (1994).

[36] Y. Kantor and M. Kardar, Phys. Rev. E **51**, 1299 (1995).

[37] A. V. Dobrynin, M. Rubinstein, and S. P. Obukhov, Macromolecules **29**, 2974 (1996).

[38] S. Minko, A. Kiriy, G. Gorodyska, and M. Stamm, J. Am. Chem. Soc. **124**, 3218 (2002).

[39] A. Kiriy, G. Gorodyska, S. Minko, W. Jaeger, P. Štěpánek, and M. Stamm, J. Am. Chem. Soc. **124**, 13454 (2002).

[40] L. J. Kirwan, G. Papastavrou, M. Borkovec, and S. H. Behrens, Nano Lett. **4**, 149 (2004).

[41] S. Lages, P. Lindner, P. Sinha, A. Kiriy, M. Stamm, and K. Huber, Macromolecules **42**, 4288 (2009).

[42] B. Xi and S.-Y. Ran, J. Polym. Sci., Part B: Polym. Phys. **55**, 971 (2017).

[43] U. Micka, C. Holm, and K. Kremer, Langmuir **15**, 4033 (1999).

[44] A. V. Lyulin, B. Dünweg, O. V. Borisov, and A. A. Darinskii, Macromolecules **32**, 3264 (1999).

[45] P. Chodanowski and S. Stoll, J. Chem. Phys. **111**, 6069 (1999).

[46] H. J. Limbach, C. Holm, and K. Kremer, Eurphys. Lett. **60**, 566 (2002).

[47] H. J. Limbach and C. Holm, J. Phys. Chem. B **107**, 8041 (2003).

[48] S. Uyaver and C. Seidel, J. Phys. Chem. B **108**, 18804 (2004).

[49] Q. Liao, A. V. Dobrynin, and M. Rubinstein, Macromolecules **39**, 1920 (2006).

[50] J. Jeon and A. V. Dobrynin, Macromolecules **40**, 7695 (2007).

[51] G. Reddy and A. Yethiraj, Macromolecules **39**, 8536 (2006).

[52] R. Chang and A. Yethiraj, Macromolecules **39**, 821 (2006).

[53] M. N. Spiteri, C. E. Williams, and F. Boué, Macromolecules **40**, 6679 (2007).

[54] W. Essafi, M.-N. Spiteri, C. Williams, and F. Boué, Macromolecules **42**, 9568 (2009).

[55] W. Essfi, A. Abdelli, G. Bouajila, and F. Boué, J. Phys. Chem. B **116**, 13525 (2012).

[56] S. B. Mahmoud, W. Essafi, A. Brûlet, and F. Boué, Macromolecules **51**, 9259 (2018).

[57] F. J. Solis and M. Olvera de la Cruz, Macromolecules **31**, 5502 (1998).

[58] G. Migliorini, N. Lee, V. Rostiashvili, and T. A. Vilgis, Eur. Phys. J. E **6**, 259 (2001).

[59] H. Tang, Q. Liao, and P. Zhang, J. Chem. Phys. **140**, 194905 (2014).

[60] R. Wang and Z.-G. Wang, Macromolecules **45**, 6266 (2012).

[61] R. Wang and Z.-G. Wang, Macromolecules **47**, 4094 (2014).

[62] G. H. Fredrickson, *The Equilibrium Theory of Inhomogeneous Polymers* (Oxford, 2006).

[63] A.-C. Shi and J. Noolandi, Macromol. Theory Simul. **8**, 214 (1999).

[64] Q. Wang, T. Taniguchi, and G. H. Fredrickson, J. Phys. Chem. B **108**, 6733 (2004).

[65] C. Tong, Y. Zhu, H. Zhang, F. Qiu, P. Tang, and Y. Yang, J. Phys. Chem. B **115**, 11307 (2011).

[66] Y.-X. Liu, H.-D. Zhang, C.-H. Tong, and Y.-L. Yang, Macromolecules **44**, 8261 (2011).

[67] I. Nakamura and Z.-G. Wang, Soft Matter **8**, 9356 (2012).

[68] C. E. Sing, J. W. Zwanikken, and M. Olvera de la Cruz, Nat. Mater. **13**, 694 (2014).

[69] R. Wang and Z.-G. Wang, J. Chem. Phys. **135**, 014707 (2011).

[70] K. J. Hou and J. Qin, Macromolecules **51**, 7463 (2018).

[71] K. Shen and Z.-G. Wang, J. Chem. Phys. **146**, 084901 (2017).

[72] Z.-G. Wang, Phys. Rev. E **81**, 021501 (2010).

[73] R. Wang and Z.-G. Wang, J. Chem. Phys. **142**, 104705 (2015).

[74] J. D. Hoffman, *Numerical Methods for Engineers and Scientists* (Marcel Dekker, 2001).

[75] M. A. Pigaleva, I. V. Portnov, A. A. Rudov, I. V. Blagodatskikh, T. E. Grigoriev, M. O. Gallyamov, and I. I. Potemkin, Macromolecules **47**, 5749 (2014).

[76] D. J. Pochan, Z. Chen, H. Cui, K. Hales, K. Qi, and K. L. Wooley, Science **306**, 94 (2004).

[77] A. Sakashita, N. Urakami, P. Ziherl, and M. Imai, Soft Matter **8**, 8569 (2012).

[78] H. Noguchi, A. Sakashita, and M. Imai, Soft Matter **11**, 193 (2015).

[79] B. A. F. Mann, K. Kremer, O. Lenz, and C. Holm, Macromol. Theory Simul. **20**, 721 (2011).

[80] M. N. Tamashiro and H. Schiessel, Macromolecules **33**, 5263 (2000).